ACS APPLIED MATERIALS & INTERFACES

Research Article

Cite This: ACS Appl. Mater. Interfaces 2020, 12, 2753−2762

www.acsami.org

Role of Multivalent Interactions in Dynamic-Template-Directed Assembly of Conjugated Polymers

Erfan Mohammadi,[†] Prapti Kafle,[†] Kai-Yu Huang,[†] Weikun Zhu,[†] Jennifer Huang,[‡] Seok-Heon Jung,[§] Jin-Kyun Lee,[§] Christopher M. Evans,[‡] and Ying Diao*[,†]

[†]Department of Chemical and Biomolecular Engineering and [‡]Department of Materials Science and Engineering, University of Illinois at Urbana-Champaign, Urbana, Illinois 61801, United States

[§]Department of Polymer Science & Engineering, Inha University, Incheon 402-751, South Korea

Supporting Information

ABSTRACT: Dynamic-template-directed assembly is a promising method to enhance molecular ordering and electronic properties of solution-coated polymer semiconductor thin films over a large area. In this work, we establish that multicomponent dynamic templates of complementary chemistries can promote polymer crystallization through cooperative multivalent interactions. We investigate this phenomenon using a combination of templating substrates including a fluoropolymer, a hydrogen-bonded liquid, and an ionic liquid (IL). Template-dependent multiscale morphology is studied by a comprehensive set of characterization techniques to understand how introducing diverse chemical moieties modulates polymer assembly. Our results clearly confirm synergistic effects between components of complementary chemistries constituting the dynamic template. The relative degree of crystallinity is improved by 50−150% for films deposited on multicomponent dynamic templates compared to their neat constituents. In addition, macroscopic alignment is increased significantly (2−5 times) compared to single-component templates. As a result, highly anisotropic charge transport is observed with apparent hole mobilities up to 3.6 $cm^2\ V^{-1}\ s^{-1}$. In contrast, such a synergistic effect is not observed when using a multicomponent dynamic template of comparable chemistries (i.e., IL and polymerized IL). We elucidate the origin of this synergistic effect by using attenuated total reflectance Fourier transform infrared spectroscopy and isothermal titration calorimetry. When the dynamic template comprises two or more components interacting with complementary binding sites on the conjugated polymer (CP) (esp. backbone vs side chain), the template−polymer interactions is significantly enhanced compared to the sum of single component contributions. These results provide valuable insights into surface-directed CP crystallization during large-area solution coating. Template dynamics is rarely studied and represents a new opportunity for guiding assembly of soft functional matter.

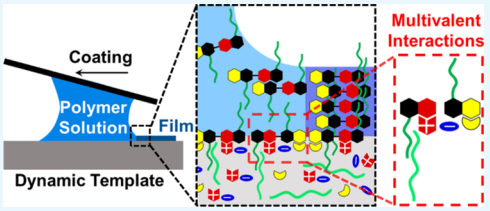

KEYWORDS: *organic semiconductors, conjugated polymers, dynamic templates, solution coating*

INTRODUCTION

Conjugated polymers (CPs) are increasingly attracting interest for their promising applications in flexible and wearable electronics during the past decade.[1] This is because of their light weight, mechanical flexibility, and cost-effective fabrication techniques.[2,3] Optoelectronic properties of printed CP thin films depend strongly on multiscale morphology parameters.[4−8] However, it is highly challenging to control all these parameters at once during high-throughput solution coating methods. As a result, printed CP thin films often suffer from low degrees of multiscale molecular ordering, leading to deteriorating electrical properties. Some of these parameters include molecular packing and paracrystallinity, mesoscale domain morphology, and macroscale polymer chain alignment.[9,10] Many variables could influence the CP assembly during solution coating such as molecular design,[8,11,12] deposition methods and conditions,[13−16] and substrate surface properties.[17−22] Specifically, substrate−polymer interactions play a critical role in the CP assembly and can offer the opportunity for multiscale morphology control across various molecular systems and processing conditions.[17,18,23] Modulating substrate−CP interactions by controlling surface chemistry[17,18,22] and nanoscale topology[19,24,25] has led to significant degrees of control on printed thin film ordering. Our recent works show that dynamic templates in the form of liquid-infused nanoporous media and polymer gels can drastically enhance polymer crystallization and alignment through promoting template−polymer interactions.[23,26,27] We define dynamic templates as substrates that facilitate crystallization by rearranging their surface structure to increase substrate-assembling media interactions. Template dynamics is a parameter seldom investigated and represents a new opportunity for guiding assembly of soft functional matter.

Received: November 19, 2019
Accepted: December 20, 2019
Published: December 20, 2019

DOI: 10.1021/acsami.9b20991
ACS Appl. Mater. Interfaces 2020, 12, 2753−2762

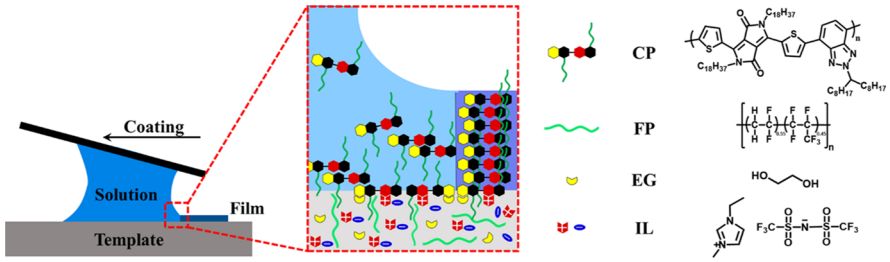

Figure 1. Dynamic templates of complementary chemistries for CP MGC. Schematic of MGC on the dynamic templates (not to scale). The arrow indicates the coating direction. Molecular structures of DPP-BTz CP, e-P(VDF:HFP) (FP), ethylene glycol (EG), and [EMIM][TFSI] (IL) are depicted.

Multivalent interaction is a key to many biological processes[28] and the assembly of complex supramolecular structures.[29,30] Multivalent binding is often cooperative as one binding event preconfigures subsequent binding events as to significantly reduce the entropic penalty of multivalent binding;[31] the overall effect is a much stronger interaction than the sum of pair-wise interaction.[32] Therefore, multivalent systems have been designed to guide an assembly of highly ordered structures not attainable from their monovalent counterparts.[33,34] Recently, we developed ion gel dynamic templates and observed an unexpected synergistic effect between components of ion gel dynamic templates promoting crystallization of CPs, outperforming templates of neat constituents.[27] Based on computational and experimental results, we ascribed this phenomenon to the complementary multivalent interactions of dynamic templates with CPs facilitated by rapid template reconfigurability. However, this hypothesis has not been tested. Further, it remains unclear what is required for multicomponent dynamic template to exhibit such synergy and whether this synergistic phenomenon is general.

In this work, we seek to directly validate the aforementioned hypothesis and to show generality of the mechanism of cooperative multivalent binding by testing a range of neat, binary, and ternary dynamic templates well beyond binary ion gels. Distinct from our previous work,[27] we further develop quantitative metrics of such synergistic phenomenon through measuring enthalpy of adsorption and develop molecular level understanding of the template−polymer interactions through spectroscopic studies. Specifically, by employing diverse chemical moieties, we expand multicomponent dynamic templates design introducing complementary binding sites for CPs to promote its crystallization. Templates are constructed from the combination of an ionic liquid (IL), a hydrogen-bonded liquid and a fluoropolymer (FP). To investigate the influence of the dynamic template on the CP thin film morphology, we carry out comprehensive characterizations including cross-polarized optical microscopy (C-POM), atomic force microscopy (AFM), ultraviolet−visible spectroscopy (UV−vis), and grazing incidence X-ray diffraction (GIXD). We observe significantly enhanced in-plane alignment and crystallinity of CP thin films when combining templates of complementary chemistries as compared to their neat counterpart. The corresponding organic field-effect transistors exhibit apparent hole mobilities reaching a value of up to 3.6 $cm^2 V^{-1} s^{-1}$. To elucidate the observed synergistic phenomenon, we perform attenuated total reflectance Fourier transform infrared (ATR−FTIR) spectroscopy to validate the multivalent nature of template−CP interactions. We further perform isothermal titration calorimetry (ITC) to show that multivalent interactions lead to enhanced enthalpy of adsorption of the CP on multicomponent dynamic template. We hypothesize that stronger template−polymer interactions due to multivalent binding promote nucleation and expedite the crystallization process leading to the observed enhancement in thin film morphology. We believe this methodology is potentially applicable to other template-directed assembly processes beyond organic electronics.

RESULTS AND DISCUSSION

Substrate Design. We studied substrate-dependent crystallization of a high-performing semi-crystalline diketopyrrolopyrrole (DPP)-based D−A polymer (DPP-BTz).[11,14] The CP thin film was deposited from the chloroform solution via meniscus-guided coating (MGC). MGC is used to resemble roll-to-roll printer characteristics[17,23,35] (Figure 1). Dynamic templates included neat and blends of a FP e-P(VDF:HFP), a hydrogen-bonded liquid ethylene glycol (EG) and an IL [EMIM][TFSI], whose chemical structures are depicted in Figure 1. These template components comprised of different chemical moieties were selected to provide different means of interactions with DPP-BTz through dipole−nonpolar, dipole−π, and ion−π interactions, respectively. Because of distinct chemistries, we surmised that different template components interact with different moieties of DPP-BTz, which we later validated by ATR−FTIR. Liquid templates [EG, IL, and their binary mixtures (EG:IL)] were constructed by infiltrating them in nanoporous AAO membranes supported by glass substrates to ensure their compatibility with MGC.[23] Gel templates including a neat FP, binary FP:IL, and ternary FP:EG:IL were prepared by spincoating from acetone solutions on plasma-treated glass substrates. It should be noted that we were unable to fabricate stable EG:FP templates because EG and the FP were not fully miscible.

Template-Dependent Multiscale Morphology of Coated Thin Films. Next, we characterized DPP-BTz thin film morphology to uncover the role of template composition in guiding crystallization during solution coating. We analyzed degree of alignment, crystallinity, and preferred molecular orientation over multiple length scales using the combination of C-POM, UV−vis, AFM, and GIXD.

Figure 2a summarizes C-POM images showing an enhanced optical birefringence of DPP-BTz thin films by diversifying the template chemical composition. In agreement with our previous reports and inferred from UV−vis and GIXD results (discussed later), the orientation of polymer backbone was perpendicular to the coating direction. Therefore, the C-POM images obtained with the coating direction oriented 0° (45°) relative to the crosspolarizer axis would be the darkest

DOI: 10.1021/acsami.9b20991
ACS Appl. Mater. Interfaces 2020, 12, 2753−2762

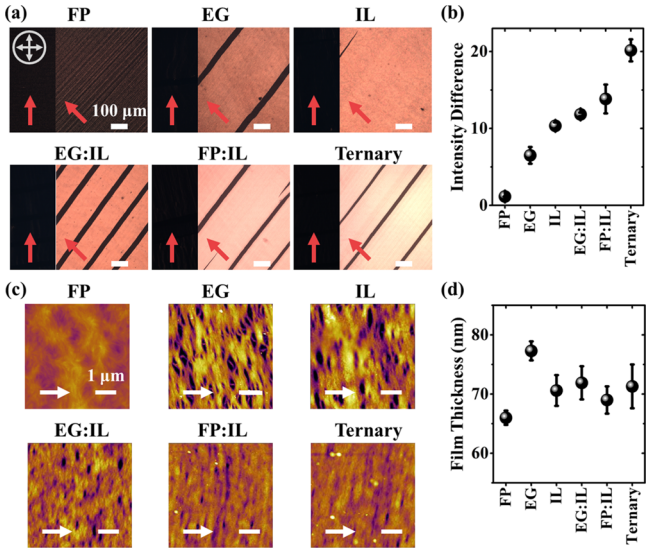

Figure 2. DPP-BTz thin film macroscale and mesoscale morphology analysis via C-POM and AFM. (a) C-POM images with the coating directions (single arrows) parallel and 45° rotated relative to the crosspolarized light. The direction of the crossed polarizers is shown using crossed arrows. All scale bars are 100 μm. Employing multicomponent dynamic templates enhanced DPP-BTz thin film birefringence. As we rotate the sample under C-POM, the image intensity uniformly changes which indicates that the film is highly ordered macroscopically. (b) The normalized average intensity difference dependent on template composition. This value is proportional to the birefringence of the polymer film and is independent of thickness because it is normalized by I_0. The cracks were excluded in the image analysis. (c) Tapping-mode AFM height images of solution-coated DPP-BTz thin films. The arrows indicate coating direction and scale bars are 1 μm. (d) Template-dependent film thickness determined from crack cross sections within the DPP-BTz thin films.

(brightest) images. To quantify thin film anisotropy from C-POM birefringence, we calculated the normalized average intensity difference of samples from $\frac{I_{45}-I_0}{I_0}$, where I_0 (I_{45}) is the average intensity of the image taken parallel (and 45° rotated) with respect to the coating direction. Polymer films with higher degree of alignment and/or crystallinity exhibited larger intensity difference, when comparing films of the same thickness. Figure 2b summarizes the template-dependent C-POM birefringence, showing that FP-templated DPP-BTz films were almost isotropic (1.1 ± 0.1), whereas films coated on EG (6.5 ± 1.1) and IL (10.3 ± 0.5) dynamic templates were highly aligned. The optical birefringence was further increased for films deposited on multicomponent dynamic templates compared to their neat constituents with the maximum intensity difference of 20.1 ± 1.4 corresponding to the ternary template. This trend consistently appeared locally evident from images obtained at higher magnifications (Figure S1). We ascribe the increase in C-POM birefringence to higher alignment and/or crystallinity of CP thin films deposited on multicomponent dynamic templates. Correspondingly, AFM images (Figure 2c) show that FP-templated films were comprised of tiny fibers exhibiting no alignment, whereas the rest of the films consisted of aligned fiber domains of hundreds of nanometers in width. Interestingly, from neat to binary and ternary dynamic templates, the voids between the fiber domains significantly decreased in both size and area density, suggesting increasing domain width and expedited domain growth rate transverse to the fiber long axis on multicomponent dynamic templates. We also determined the film thicknesses via AFM measurements to be in the range of 70 ± 5 nm across the template series (Figure 2d). Thus, film thickness would not interfere with our multiscale morphology analysis.

We next confirmed the superior in-plane alignment of CP films deposited on multicomponent templates via polarized UV−vis measurements. This technique also revealed polymer conformation change coupled with enhanced in-plane alignment. Figure 3a summarizes the normalized UV−vis absorption spectra for the solution-coated DPP-BTz thin

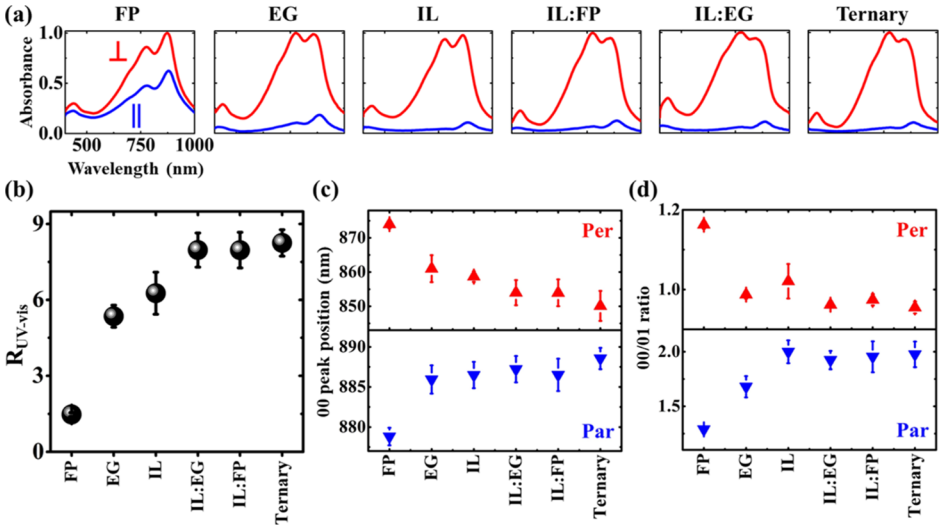

Figure 3. UV−vis measurements of substrate-dependent DPP-BTz thin films. (a) Normalized polarized UV−vis absorption spectra of DPP-BTz films coated on single- and multi-component dynamic templates measured when the film coating direction is parallel "∥" (blue) or perpendicular "⊥"(red) to the axis of the polarizer. (b) (0−0) peak dichroic ratio as a function of template composition. (c) 0−0 peak position and (d) 0−0 to 0−1 vibronic peak ratio as a function of template composition measured with the coating direction parallel (blue) and perpendicular (red) to the polarizer axis.

DOI: 10.1021/acsami.9b20991
ACS Appl. Mater. Interfaces 2020, 12, 2753−2762

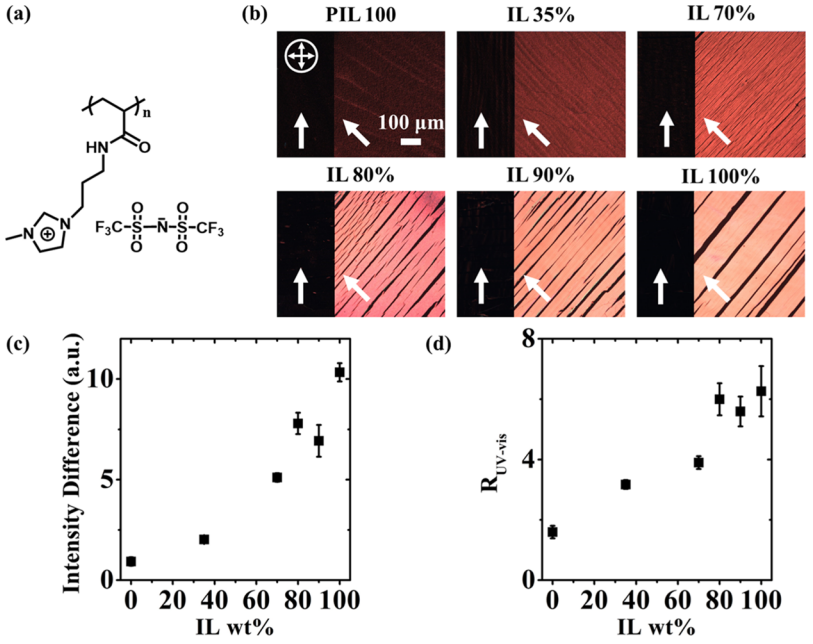

Figure 4. DPP-BTz thin film morphology coated on PIL:IL binary templates. (a) PIL molecular structure. (b) C-POM images with the coating directions oriented at 0 and 45° with respect to the crosspolarized light. The scale bars are 100 μm. Crossed arrows show the orientation of the crossed polarizers. (c) The average intensity difference extracted from C-POM images and (d) UV−vis dichroic ratio as a function of template composition. No synergy is observed for the PIL:IL binary template, regardless of IL wt %.

films, while the polarizer axis oriented parallel and perpendicular to the coating direction. Greater perpendicular absorbance spectra suggested that polymer backbones assemble orthogonally to the coating direction. This is because the largest component of the optical transition dipole is expected to be along the long axis of the conjugated backbone.[14,36,37] The in-plane alignment of the CP thin film was quantified by the 0−0 vibronic peak dichroic ratio comparing the intensity of the polarized UV−vis spectra parallel (I_{par}) and perpendicular (I_{per}) to the coating direction: $R_{UV-vis} = I_{per}/I_{par}$. As expected R_{UV-vis} was close to unity (1.5 ± 0.1) for the neat FP-templated films and significantly increased on dynamic templated films reaching 5.3 ± 0.4 and 6.3 ± 0.8 for EG and IL templated films, respectively. All three multicomponent dynamic templates exhibited higher R_{UV-vis} compared to the neat templates with the ternary system having the highest value of 8.2 ± 0.5. It is important to note that R_{UV-vis} would result in lower limit for the degree of alignment because the polymer chain might be slightly curved in solid-state even for rigid DPP-based CPs.[36,37] These results further confirm the synergy between components of the binary and ternary templates and allude to the role of multivalent binding in promoting CP crystallization. Concurrent with the enhanced uniaxial in-plane alignment by enriching template chemistry, we observed signatures of enhanced H-aggregation in perpendicular and J-aggregation in the parallel scans. In the perpendicular (parallel) spectra the 0−0 peak position exhibited a blue (red) shift from 874 to 850 nm (879 to 889 nm), and 0−0/0−1 peak ratio changed from 1.2 to 0.9 (1.3 to 2.0).[38] Overall, UV−vis measurements suggest higher in-plane alignment in films coated on multicomponent templates. How can multicomponent dynamic templates induce domain alignments in CP films? We hypothesize that multicomponent dynamic templates enhance interactions with CPs via multivalent interactions (discussed below). Such enhanced interactions would enrich CPs near the template surface[23] thereby expediting nucleation of polymer fibers. The earlier the nucleation, the longer the polymer fibers would grow and the easier they will be aligned by the printing flow; we reported printing flow induced alignment of CPs in earlier works.[35,39] In other words, we ascribe the polymer alignment to the compound effect of enhanced polymer nucleation on multicomponent dynamic templates and coating-flow-induced alignment of nucleated polymer fibers.

We further showed that complementary chemistry is necessary for observing such synergy in multicomponent systems by using a polymerized IL (PIL) with imidazole pendant group tethered to the backbone.[40] The PIL structure is shown in Figure 4a, which has a glass transition temperature comparable to the FP (∼−20 °C) and chemistry comparable to IL. Because of similar chemistry between PIL and IL, the PIL:IL mixture served as a negative control for the FP:IL, which exhibit complementary chemistry between the FP with highly polar groups and IL with ionic moieties. C-POM images for DPP-BTz films printed on template series with varying PIL to IL ratio is summarized in Figure 4b. In contrast to the FP:IL case that showed higher birefringence and UV−vis dichroic ratio than the neat IL template, we observed no synergy between PIL and IL. Specifically, when PIL was mixed into IL, both optical birefringence (Figure 4c) and UV−vis dichroic ratio (Figure 4d) monotonically decreased with an increase in the PIL content or a decrease in the IL content. In comparison, when the FP was added into IL, both optical birefringence (Figure 2b) and UV−vis dichroic ratio (Figure 3b) increased instead. This observation suggests that it is necessary for the multicomponent templates to have complementary chemical moieties interacting with the assembling CP to exhibit synergistic templating effects.

Next, we used GIXD to assess template-dependent in-plane and out-of-plane molecular orientation within crystalline domains of the polymer thin film. Our $\pi-\pi$ stacking peak analysis demonstrated that the highest relative degree of

DOI: 10.1021/acsami.9b20991
ACS Appl. Mater. Interfaces 2020, 12, 2753−2762

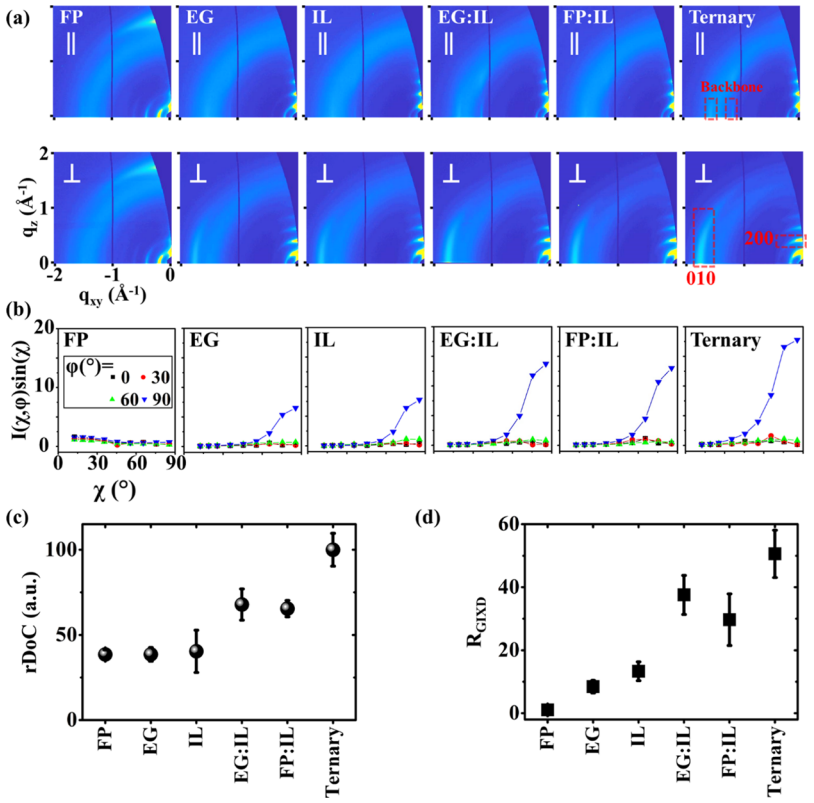

Figure 5. GIXD characterizations of DPP-BTz films coated on various templates. (a) GIXD diffraction patterns with the incidence beam parallel (top) and perpendicular (bottom) to the coating direction. (010) and (200) peaks are labeled. (b) Geometrically corrected intensities of $\pi-\pi$ stacking (010) peaks as a function of the polar angle (χ) and substrate in-plane rotation angle (φ) for films deposited on different templates. We transferred DPP-BTz films to ODTS-treated SiO_2 to directly compare across templates. We carried out the measurements at $\varphi = 0°$ (parallel), 30°, 60°, and 90° (perpendicular). (c) rDoC obtained by integrating the $\pi-\pi$ stacking peak intensity over χ and φ. Error bars are from (010) peak multipeak fitting. (d) GIXD dichroic ratio of "edge-on" $\pi-\pi$ stacking peaks for DPP-BTz polymer thin films dependent on the template chemical composition. FP-coated films were isotropic in-plane ($R_{GIXD} \approx 1$), whereas dynamic template-coated films were highly anisotropic ($R_{GIXD} \gg 1$). Ternary template showed the highest R_{GIXD} exceeding 50.

crystallinity (rDoC) and alignment was obtained using the multicomponent dynamic templates. Figure 5a summarizes the GIXD diffraction patterns measured parallel and perpendicular to the coating direction across template series. The corresponding $\pi-\pi$ and lamellar stacking distances are shown in Figure S2. FP-templated films exhibited preferential "face-on" orientation, whereas films coated on dynamic templates show predominantly "edge-on" stacking. We next extracted pole figures to quantify the orientation distribution of π-crystallites (Figure 5b). We plotted the geometrically corrected, thickness-normalized $\pi-\pi$ stacking peak (010) intensities as a function of polar angle (χ) and substrate in-plane rotation angle (φ). These pole figures demonstrated that FP-templated films adopted a "face-on" orientation and were almost isotropic in-plane. On the other hand, all films coated on dynamic templates exhibited "edge-on" orientation and pronounced in-plane alignment. We further calculated the rDoC of DPP-BTz thin films by integrating the geometrically corrected peak intensities over χ and φ[17] (Figure 5c). Compared to neat templates, the rDoC values for films coated on binary dynamic templates were increased by >62%. Further enriching the template chemistry, using ternary template, enhanced rDoC by up to 150% compared to the neat templates. This observation is consistent with the trend observed from C-POM birefringence (Figure 2); both indicate that multicomponent dynamic templates have higher crystallinity.

Besides crystallinity, we also quantitatively compared in-plane alignment dependent on template composition. For dynamic templates, an "edge-on" $\pi-\pi$ stacking peak was stronger for perpendicular scans. This corresponds to the preferred backbone alignment orthogonal to the coating direction (observed from UV−vis as well). To quantify the in-plane molecular alignment, we compared the normalized peak areas of "edge-on" ($83° < \chi < 88°$) $\pi-\pi$ stacking peak with the incidence beam parallel ($A_{\parallel}$) and perpendicular ($A_{\perp}$) to the coating direction and calculated the GIXD dichroic ratio: $R_{GIXD} = A_{\perp}/A_{\parallel}$ (Figure 5d). From neat to binary dynamic templates, R_{GIXD} drastically increased from 8.4 ± 2.0 (EG) and 13.3 ± 3.0 (IL) to 37.5 ± 6.2 (IL:EG) and 29.7 ± 8.2 (IL:FP). The highest value was obtained from films coated on the ternary dynamic templates to yield $R_{GIXD} = 50.6 \pm 7.5$, corroborating the C-POM and UV−vis results. Higher R_{GIXD} compared to R_{UV-vis} is because GIXD only probes the crystalline domains and not amorphous portions of the film; besides, UV−vis gives the lower limit of the alignment as discussed previously. At $q_{xy} \approx 1.15$ and 1.52 Å^{-1} we observed two peaks, ascribed to the backbone repeat unit,[14] which progressively became more intense from the neat to multicomponent templates. This may have also arisen from enhanced molecular ordering and reduced paracrystalline disorder that produced constructive interference from the backbone repeat units. In summary, as chemical composition of the template became more diverse, molecular ordering of

DOI: 10.1021/acsami.9b20991
ACS Appl. Mater. Interfaces 2020, 12, 2753−2762

the solution-coated DPP-BTz thin films improved in terms of both crystallinity and alignment.

Morphology-Dependent Field-Effect Transistor Performance. We fabricated field-effect transistors to establish the interplay between the CP thin film morphology and charge transport properties. Overall, we observed superior and anisotropic charge carrier mobilities for highly ordered films. Bottom-gate top-contact FETs were fabricated with the active channel oriented parallel and perpendicular to the coating direction (Figure 6a). We transferred solution-coated DPP-BTz films to ODTS-SiO_2/Si substrates chosen because of their low interfacial trap densities[41] to allow direct morphology comparison across templates (see Methods for fabrication details). The favorable carrier transport direction is quantified by apparent hole mobilities (μ_{app}) in the saturation regime measured parallel and perpendicular to the coating direction (Figure 6b). The representative transfer, gate voltage (V_{GS})-dependent μ_{app}, and output plots and key FET parameters are summarized in Figure S3 and Table S1. Transfer curves did not show nonideal "kinks" reported for high-performing devices,[42] and the average reliability factor[43] was >65.5%.

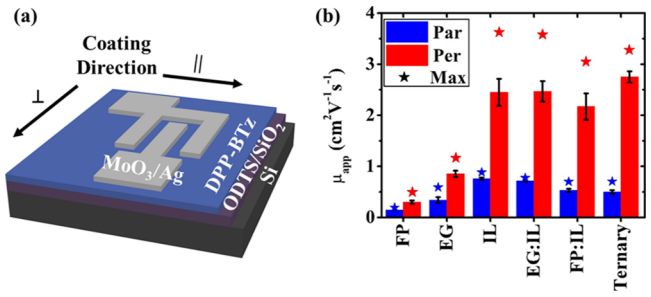

Figure 6. Charge transport property characterizations using FET configuration. (a) FET device schematic with bottom-gate top-contact configuration with the conductive channel parallel (||) and perpendicular (⊥) to the coating direction. (b) Template-dependent μ_{app} extracted from saturation regime at V_{DS} = −100 V. At least 10 devices were measured from which the standard deviation is calculated.

Figure 6b shows that μ_{app} values increase >2 times from FP-templated films to EG-templated ones in both parallel and perpendicular directions. FETs fabricated from DPP-BTz films deposited on ILs and multicomponent dynamic templates exhibited much higher μ_{app} compared to those of FPs and EG. Highest average hole mobility of 2.75 ± 0.11 cm^2 V^{-1} s^{-1} and largest charge transport anisotropy of 5.53 ± 0.47 were obtained from films deposited on the ternary template. The average hole mobility was higher perpendicular to the coating direction than parallel, indicating that the preferred hole transport is intrachain. The highest measured μ_{app} surpassed 3.61 cm^2 V^{-1} s^{-1}. Increase in charge carrier mobility is mainly attributed to enhanced crystallinity and in-plane alignment. It should be noted that μ_{app} values in the current work are not comparable to our previous publication[27] because thin film morphology and thickness are not the same because of modified solution coating conditions.

Quantifying Template−CP Interactions. Our comprehensive multiscale morphology analysis showed that as template chemistry become enriched, DPP-BTz thin film molecular ordering significantly increased. We hypothesize that this is a result of enhanced CP−template interactions by adding complementary chemical moieties to the dynamic template. Stronger CP−template interactions can expedite polymer crystallization by promoting surface-induced nucleation. To test this hypothesis, we carried out ATR−FTIR spectroscopy and ITC. We used ATR−FTIR to investigate whether various chemical moieties present different binding sites to the CP; this serves to validate the multivalency of the CP−template interactions and to elucidate the role of complementary chemistries. We employed ITC to quantify the CP−template interactions in terms of enthalpy of adsorption of the CP onto the template.

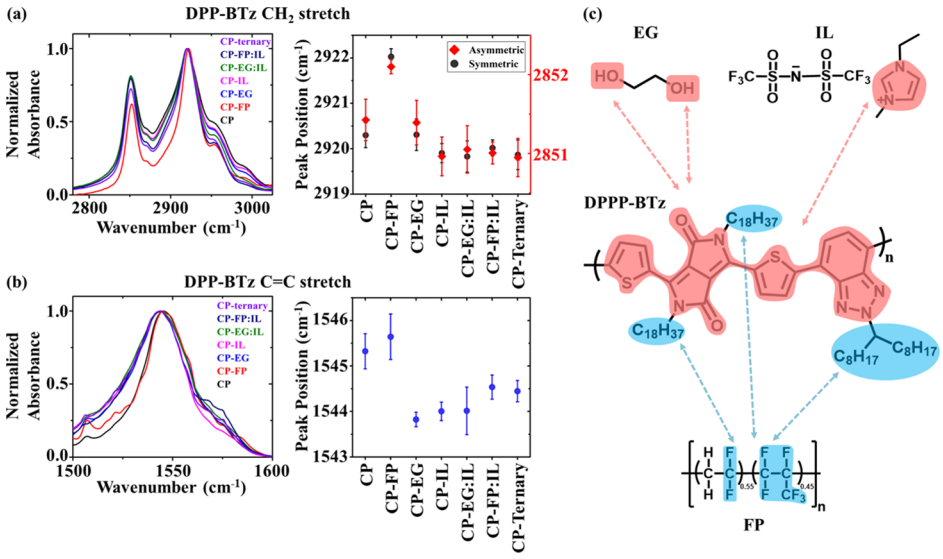

Figure 7. ATR−FTIR spectroscopy to quantify specific interactions between DPP-BTz and templates. Absorbance spectra of DPP-BTz (a) alkyl side chain CH_2 symmetric and asymmetric stretching and (b) backbone C=C asymmetric stretching and their corresponding peak shift as a function of template composition. Characteristic peaks are chosen to have the least interference from peaks of other components. (c) Schematic of molecular structures of DPP-BTz and template components illustrating that the FP mainly interact with the alkyl side chains while EG and IL interact with the conjugated backbone.

DOI: 10.1021/acsami.9b20991
ACS Appl. Mater. Interfaces 2020, 12, 2753−2762

Samples for ATR−FTIR were prepared by blending the DPP-BTz solution and each template to the level of saturation and then forming a film by drop casting (see Experimental sections for sample preparation details). The full spectra for measured samples are summarized in Figure S4. First, we focused on two regions in the DPP-BTz spectrum: (i) symmetric and asymmetric CH_2 stretching peaks (2850−2925 cm^{-1}) associated with the alkyl side chains (Figure 7a) and (ii) asymmetric C═C stretching peaks (1543−1546 cm^{-1}) of the conjugated backbone[44] (Figure 7b). While side chain CH_2 stretching peaks were shifted to higher wavenumbers in the presence of FPs, other templates had negligible influence on the peak shape and position. Contrarily, the backbone C═C peaks were shifted to lower wavenumbers for all templates except the FP. These observations suggest that the FP mainly interact with the CP side chains but EG and IL interact with the conjugated backbone (Figure 7c). Next, we turned our attention to the characteristic absorption peaks of the templates to understand which specific chemical moieties were engaged in their interaction with the CP (Figure S5a−d). We observed that chemical moieties involving electronegative atoms in the FP and EG (fluorine and oxygen) experienced peak shifts. Based on Figure S5, FP CF_2 stretch (1130−1180 cm^{-1}) and EG O−H stretching peak (3300−3310 cm^{-1})[45] showed clear peak shifts. In addition, IL cation imidazole C−H (3105−3165 cm^{-1}) and IL anion SNS peaks (1030−1055 cm^{-1}) moved to higher frequency showing favorable interactions of both charged species of IL with the CP;[46] however, the extent of peak shift is much less for anion compared to that of cation. It should be noted that the extent of peak shift is irrelevant to these results because we cannot control the amount of template miscible with the CP solution. These peak shifts were ascribed to the change in chemical environments of corresponding stretching modes due to favorable interactions between templates and the CP. In summary, ATR−FTIR measurements inform favorable interaction between DPP-BTz alkyl side chains and FPs and strong interaction between DPP-BTz conjugated backbone with EG and IL. We hypothesize that employing multicomponent dynamic templates of complementary chemistries can enhance template−CP interactions through multivalent binding.

We then employed ITC to directly measure DPP-BTz adsorption enthalpy (ΔH_{net}) to the template which is a direct measure of the strength of interactions. Similar to our recent work,[26] a single-injection experiment was used where one drop of DPP-BTz solution is spread onto the template. ΔH_{net} was determined by subtracting the released heat on titrating DPP-BTz solution and pure solvent on various templates (Figures 8 and S6). All templates exhibited favorable interactions with DPP-BTz ($\Delta H_{net} < 0$). As expected, IL has the strongest interaction among the neat templates, given the strong interactions between the IL cation and the CP backbone through electrostatic forces and ion−π interactions inferred from FTIR in this work and from MD simulations and ^{1}H NMR measurements in our previous work.[23] The interaction between DPP-BTz and multicomponent dynamic templates is much stronger than the neat templates (>45% higher ΔH_{net} compared to IL). We attribute this to introduce complementary sites for template−CP binding suggested by ATR−FTIR measurements. As a result of stronger interaction, the CP would concentrate near the dynamic template leading to a lower free energy barrier to nucleation and expedited crystallization process. This result is consistent with our observations that the extent of molecular ordering in films printed on multicomponent dynamic templates was significantly higher than the neat templates. It should be emphasized that, herein, template reconfigurability plays a vital role in maximizing favorable interactions and promoting CP crystallization.[23,26]

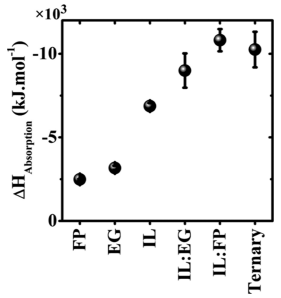

Figure 8. ITC measurements to quantify the interaction between DPP-BTz and dynamic templates. We calculated the net enthalpy of adsorption (ΔH_{net}) from subtracting the released heat during titrating the neat solvent from that of polymer solution. The strength of template−CP interactions is proportional to ΔH_{net}.

CONCLUSIONS

In conclusion, we designed dynamic templates capable of strong multivalent interactions with CP molecules during large-area solution coating. This was achieved by diversifying active binding sites involved in CP−surface interactions by employing multicomponent dynamic templates of complementary chemistries. The multicomponent templates studied included neat or mixture of a FP, a hydrogen-bonded liquid (EG) and an IL. We studied the template-dependent multiscale morphology of solution coated DPP-BTz thin films using a combination of C-POM, UV−vis, AFM, and GIXD. Our results suggested that DPP-BTz films coated on multicomponent templates had significantly higher degree of crystallinity and alignment compared to their neat counterparts with maximum values obtained on the ternary template. DPP-BTz films deposited on the ternary template exhibited over two-fold increase in C-POM birefringence (intensity difference > 21) and 4-fold increase in the GIXD dichroic ratio (R_{GIXD} > 51). UV−vis showed a significantly improved in-plane alignment with R_{UV-vis} reaching 9 in DPP-BTz thin films coated on multicomponent templates. GIXD was also used to determine rDoC showing the maximum value for the ternary template which was >150% higher than single-component templates. As a result of superior molecular ordering of dynamic-templated films, hole mobilities measured in field-effect transistors exceeded 0.9 and 3.6 $cm^2\ V^{-1}\ s^{-1}$ when active channels oriented parallel and perpendicular to the coating direction. Highest average mobilities and charge transport anisotropy were observed in films coated on the ternary dynamic templates. We attribute the higher molecular order of DPP-BTz thin films coated on multicomponent dynamic templates to stronger template−polymer interactions owing to multivalent binding, which we validated via a combination of ATR−FTIR and ITC. ATR−FTIR measurements showed that the FP mainly interacts with the alkyl side chains of DPP-BTz while EG and IL interactions is predominantly through the conjugated backbone. We further used ITC to directly quantify CP−template interactions and observed the highest enthalpy of binding of DPP-BTz on multicomponent dynamic

DOI: 10.1021/acsami.9b20991
ACS Appl. Mater. Interfaces 2020, 12, 2753−2762

templates. This validated our hypothesis that multicomponent dynamic templates with complementary chemistries serve to enhance CP−template interactions. We reason that strong multivalent interactions reduce the DPP-BTz nucleation-free energy barrier, which result in an expedited crystallization process. The synergy between faster crystallization and flow-induced alignment during MGC led to improved degree of alignment and crystallinity of solution-coated CP thin films. This concept can potentially be applied to direct molecular assembly of other systems beyond organic electronics, because of the significance of interfacial properties during crystallization.

EXPERIMENTAL METHODS

Dynamic Template Preparation. We constructed liquid templates by infiltrating nanoporous membranes supported by glass substrates to form a semi-solid substrate compatible with large-scale solution coating as described in previous reports.[23,26] The pore size and diameter of AAO membranes were 200 and 1.3 mm, respectively. Liquid templates include ethylene glycol (EG) (99.8% anhydrous purchased from Sigma-Aldrich), 1-ethyl-3-methylimidazolium bis-(trifluoromethylsulfonyl)imide ([EMIM][TFSI]) (≥98% purchased from Solvionic), and EG:IL binary template. Both EG and IL were stored in a nitrogen glovebox prior to use as received. The EG:IL binary template was prepared by mixing 20 wt % EG and 80 wt % [EMIM][TFSI] for >3 h at room temperature before infiltrating in AAO supported by glass substrates.

To prepare ion gel dynamic templates, we first dissolved the polyvinylidene fluoride-*co*-hexafluoropropylene e-P(VDF:HFP) with VDF to a HFP molar ratio of 55:45 (Dyneon Fluoroelastomer FE purchased from 3M Company) in acetone (Optima grade, Fisher Scientific) at room temperature stirring for >3 h. Next, we added IL or EG:IL mixture to the e-P(VDF:HFP) solution and stirred for >2 h to ensure full dissolution. e-P(VDF:HFP) and acetone weight ratios were fixed at 1:8. For binary and ternary gel templates [EMIM]-[TFSI], EG weight was controlled to make a 1:9 weight ratio of e-P(VDF:HFP)/[EMIM][TFSI] (FP:IL) and a 1:2:7 weight ratio of e-P(VDF:HFP)/EG/[EMIM][TFSI] (FP:EG:IL). We used on-the-fly-dispensing method[47] to spin cast the resulting solution on plasma-treated glass substrates at 2500 rpm for 1 min. We dried the substrates overnight without further annealing in the nitrogen environment. We avoided annealing the ternary templates at high temperatures to avoid evaporation of EG from the ternary templates. PIL was synthesized as previously reported.[40]

CP Thin Film Fabrication. Poly[[2,5-bis(2-octadecyl)-2,3,5,6-tetrahydro-3,6-diketopyrrolo[3,4-*c*]pyrrole-1,4-diyl]-*alt*-(2-octylnonyl)-2,1,3-benzotriazole] (DPP-BTz) (M_n = 176 kg·mol^{-1} and PDI = 2.5) was synthesized as reported before.[11,14] DPP-BTz was dissolved in anhydrous chloroform (Macron ACS grade) to prepare 5.0 mg·mL^{-1} solution. To ensure that all the polymers are dissolved, the solution was stirred >3 h until a clear homogeneous solution was obtained. A MGC method was used to cast DPP-BTz thin films with details reported before.[23] The substrate temperature was fixed at 25 °C and the speed of the blade was set at 0.25 mm·s^{-1}. We confirmed experimentally that all templates were practically immiscible with the CP ink solution during the fast solution coating process.

For C-POM, AFM, and GIXD measurements, as-coated polymer films were transferred to ODTS-functionalized silicon wafer with 300 nm thermally grown SiO_2 by the following procedure (see previous reports[17,23] for ODTS modification details). For films coated on dynamic liquid templates, first, the CP/liquid/AAO hybrid was placed upside down on the ODTS substrate. Then, plenty of an inert liquid (EG) or deionized water was added on the top to enforce the CP film attachment to the ODTS substrate. After >5 min the AAO membrane was delicately removed and the transferred films were subsequently immersed in acetonitrile for at least 5 min to remove the residual liquids. For FPs and gel templates, we followed the method established in our previous work.[27] Therefore, ODTS-modified SiO_2 was the common substrate for direct comparison of all morphology and device characterizations.

DPP-BTz Thin Film Morphology Characterizations. A Nikon Ci-POL crossed polarized optical microscope was used for visualizing DPP-BTz thin films and observing the optical birefringence. Samples were centered on a microscope stage so that the obtained images correspond to the same area while the stage was rotated. To quantify the polymer film alignment, we calculated the normalized average intensity difference by comparing the intensity of C-POM images oriented parallel and 45° rotated relative to the polarizer axis using "ImageJ" software.[48] Solid-state transmission UV−vis spectroscopy measurements were carried out at room temperature via an Agilent Cary 60 UV−Vis spectrometer. The incident light was polarized vertically via a broadband sheet polarizer. As-coated films on various templates were scanned within the wavelength of 400−1000 nm followed by manually subtracting template background spectra. To determine polymer chain alignment, UV−vis spectra were recorded with the coating direction parallel and perpendicular to the polarizer axis. Tapping mode AFM measurements were carried out using an Asylum Research Cypher instrument (Asylum Research) to assess the solution-coated DPP-BTz thin film mesoscale morphology and determining the corresponding film thickness. GIXD was performed at the small-wide-angle X-ray scattering beamline 8-ID-E using the Advanced Photon Source (Argonne National Laboratory) with an X-ray wavelength of 1.6871 Å (E_{beam} = 10.92 keV) at a 208 mm sample-to-detector distance.[49] For further details on GIXD measurements and data analysis refer to previous reports.[17,23,26,27]

FET Fabrication and Electrical Characterization. We fabricated bottom-gate top-contact FETs by transferring the as-coated DPP-BTz thin films (semiconducting layer) to a highly n-doped Si (gate) with thermally grown 300 nm SiO_2 modified by ODTS (dielectric layer) to minimize interfacial charge traps.[41] Source and drain electrodes included 8 nm thick MoO_3 and 35 nm thick silver that were thermally evaporated onto the CP films through a shadow mask. The channel length (L) was 47 ± 2 μm and width (W) was 840 ± 15 μm. All measurements were performed in the inert environment of a nitrogen glove box (room temperature) via a Keysight B1500A semiconductor parameter analyzer. The field-effect hole mobilities (μ_{app}) in the saturation regime were calculated from $I_{DS} = \frac{WC_i\mu_{app}}{2L}(V_{GS} - V_{th})^2$, where I_{DS} is the drain−source current, C_i is the dielectric capacitance per unit area (11 nF/cm^2 for ODTS-treated 300 nm SiO_2 dielectric), V_{GS} is the gate voltage, μ is the apparent carrier mobility, and V_{th} is the threshold voltage. At least 10 independent devices were used to obtain average μ_{app} values.

FTIR Spectroscopy. FTIR measurements were conducted using a Nicolet iS5 FTIR spectrometer at ambient temperature in the range of 400−4000 cm^{-1} with a wavenumber resolution of 1 cm^{-1} (step size of <0.5 cm^{-1}). Samples were prepared by mixing the neat single-component templates or acetone solution of various multicomponent templates with chlorobenzene solution of 5 g·L^{-1} DPP-BTz for >3 h while stirring. We added the DPP-BTz solution in excess to make sure we capture CP characteristic peaks reliably. As the level of miscibility for each solution was different, we then stopped stirring the solutions, allowed the mixture to settle, and extracted the homogenous (completely mixed) solution for the sample preparation. Then, we drop cast the resulting solution on a gold-coated corning glass substrate and heated up the samples at ∼50 °C to completely remove the residual solvent. The outcoming template−CP blend film was stored in an inert environment (N_2) and used for the final measurements. It should be noted that extra care was taken to ensure that samples are not exposed to ambient conditions in order to prevent appearance of additional peaks (possibility due to water and CO_2 adsorption and sample degradation) in the final spectra. The major peaks were identified using OMNIC software (Nicolet Instruments Corp.), and when fitting was necessary to find the peaks center, Igor Pro software was employed.

ITC Measurements. ITC experiments were carried out using a Nano ITC Low Volume isothermal titration calorimeter (TA Instruments) at room temperature. The data were extracted from

DOI: 10.1021/acsami.9b20991
ACS Appl. Mater. Interfaces 2020, 12, 2753−2762

NanoAnalyze software and analyzed via Origin software. Reaction cell was rigorously cleaned with a series of NaOH, formic acid, deionized water, isopropanol, chloroform, and acetone and then heated to 60 °C for >3 h to evaporate residual solvents. For liquid templates, first, 50 μL of the liquid templates was injected with a long needle into the reaction and the reference cell. We then waited for >15 min to make sure that the liquids descend completely to the bottom; no residual liquid is stuck to the walls and no bubbles formed. For FPs, IL:FP, and ternary templates, we injected their acetone solution to the cells and controlled the amount to be comparable to liquid templates after solvent was evaporated. To remove solvent, the cell was heated to 40 °C for >30 min. Next, 50 μL of 5 $g{\cdot}L^{-1}$ DPP-BTz solution in chloroform was loaded to the injection syringe and mounted on the ITC instrument. We started all titration experiments with a 0.25 μL to avoid bubbles in the main experiment. After 30 min, 3 μL of the DPP-BTz solution was titrated on the liquid template. We then recorded heat flow as a function of time ($\mu J{\cdot}s^{-1}$) for 60 min and repeated the experiment at least 3 times for each template. For further details on the experimental method and data analysis see the reference.[26]

■ ASSOCIATED CONTENT

Supporting Information

The Supporting Information is available free of charge at https://pubs.acs.org/doi/10.1021/acsami.9b20991.

Mesoscale morphology by C-POM; GIXD peak analysis; FET key properties and parameters summary; ATR–FTIR spectra and peak analysis; ITC data (PDF)

■ AUTHOR INFORMATION

Corresponding Author

*E-mail: yingdiao@illinois.edu.

ORCID

Weikun Zhu: 0000-0002-0828-3645

Jin-Kyun Lee: 0000-0001-9468-5749

Christopher M. Evans: 0000-0003-0668-2500

Ying Diao: 0000-0002-8984-0051

Author Contributions

E.M. and Y.D. designed the research project and Y.D. supervised the project. E.M. carried out the experiments and analyzed all the corresponding data. P.K. performed the GIXD measurements and E.M. analyzed the data. K.-Y.H. helped with FTIR measurements. W.Z. helped with sample preparations. J.H. and C.M.E. helped with synthesizing PIL. Semiconducting polymer synthesis was done by J.-K.L. and S.-H.J. All authors discussed, revised, and approved the manuscript.

Notes

The authors declare no competing financial interest.

■ ACKNOWLEDGMENTS

This work was funded primarily by the National Science Foundation, NSF DMR award #18-47828. E.M. and P.K. acknowledge partial support by the NSF IMRSEC: Illinois Materials Research Center under grant number DMR 17-20633. Y.D. acknowledges support from the Jiangsu Industrial Technology Research Institute (JITRI) through the JITRI International Fellowship Program. P.K. acknowledges AAUW International Fellowship. This research used resources of the Advanced Photon Source, a U.S. Department of Energy (DOE) Office of Science User Facility operated for the DOE Office of Science by Argonne National Laboratory under contract no. DE-AC02-06CH11357. We appreciate help from beamline scientist Strazalka Joseph W. of Advanced Photon Source, Argonne National Laboratory facilitating the GIXD measurements. Part of this research was performed in the Frederick Seitz Materials Research Laboratory Central Facilities, University of Illinois. Thanks to Professor Chao Wang from Chemistry department at the University of California at Riverside for kindly providing the fluoropolymer e(PVDF:HFP).

■ REFERENCES

(1) Reynolds, J. R.; Thompson, B. C.; Skotheim, T. A. *Conjugated Polymers: Properties, Processing, and Applications*, 4th ed.; CRC Press: Boca Raton, 2019.

(2) Zhang, Z.; Liao, M.; Lou, H.; Hu, Y.; Sun, X.; Peng, H. Conjugated Polymers for Flexible Energy Harvesting and Storage. *Adv. Mater.* **2018**, *30*, 1704261.

(3) Xu, J.; Wu, H.-C.; Zhu, C.; Ehrlich, A.; Shaw, L.; Nikolka, M.; Wang, S.; Molina-Lopez, F.; Gu, X.; Luo, S.; Zhou, D.; Kim, Y.-H.; Wang, G.-J. N.; Gu, K.; Feig, V. R.; Chen, S.; Kim, Y.; Katsumata, T.; Zheng, Y.-Q.; Yan, H.; Chung, J. W.; Lopez, J.; Murmann, B.; Bao, Z. Multi-scale ordering in highly stretchable polymer semiconducting films. *Nat. Mater.* **2019**, *18*, 594–601.

(4) Himmelberger, S.; Salleo, A. Engineering semiconducting polymers for efficient charge transport. *MRS Commun.* **2015**, *5*, 383–395.

(5) Dong, H.; Hu, W. Multilevel Investigation of Charge Transport in Conjugated Polymers. *Acc. Chem. Res.* **2016**, *49*, 2435–2443.

(6) Patel, B. B.; Diao, Y. Multiscale assembly of solution-processed organic electronics: the critical roles of confinement, fluid flow, and interfaces. *Nanotechnology* **2018**, *29*, 044004.

(7) Molina-Lopez, F.; Wu, H.-C.; Wang, G.-J. N.; Yan, H.; Shaw, L.; Xu, J.; Toney, M. F.; Bao, Z. Enhancing Molecular Alignment and Charge Transport of Solution-Sheared Semiconducting Polymer Films by the Electrical-Blade Effect. *Adv. Electron. Mater.* **2018**, *4*, 1800110.

(8) Hambsch, M.; Erdmann, T.; Chew, A. R.; Bernstorff, S.; Salleo, A.; Kiriy, A.; Voit, B.; Mannsfeld, S. C. B. Increased charge carrier mobility and molecular packing of a solution sheared diketopyrrolopyrrole-based donor-acceptor copolymer by alkyl side chain modification. *J. Mater. Chem. C* **2019**, *7*, 3665–3674.

(9) Noriega, R.; Rivnay, J.; Vandewal, K.; Koch, F. P. V.; Stingelin, N.; Smith, P.; Toney, M. F.; Salleo, A. A General Relationship between Disorder, Aggregation and Charge Transport in Conjugated Polymers. *Nat. Mater.* **2013**, *12*, 1038.

(10) Venkateshvaran, D.; Nikolka, M.; Sadhanala, A.; Lemaur, V.; Zelazny, M.; Kepa, M.; Hurhangee, M.; Kronemeijer, A. J.; Pecunia, V.; Nasrallah, I.; Romanov, I.; Broch, K.; McCulloch, I.; Emin, D.; Olivier, Y.; Cornil, J.; Beljonne, D.; Sirringhaus, H. Approaching disorder-free transport in high-mobility conjugated polymers. *Nature* **2014**, *515*, 384.

(11) Gruber, M.; Jung, S.-H.; Schott, S.; Venkateshvaran, D.; Kronemeijer, A. J.; Andreasen, J. W.; McNeill, C. R.; Wong, W. W. H.; Shahid, M.; Heeney, M.; Lee, J.-K.; Sirringhaus, H. Enabling high-mobility, ambipolar charge-transport in a DPP-benzotriazole copolymer by side-chain engineering. *Chem. Sci.* **2015**, *6*, 6949–6960.

(12) Son, S. Y.; Lee, G.-Y.; Kim, S.; Park, W.-T.; Park, S. A.; Noh, Y.-Y.; Park, T. Control of Crystallite Orientation in Diketopyrrolopyrrole-Based Semiconducting Polymers via Tuning of Intermolecular Interactions. *ACS Appl. Mater. Interfaces* **2019**, *11*, 10751–10757.

(13) Bucella, S. G.; Luzio, A.; Gann, E.; Thomsen, L.; McNeill, C. R.; Pace, G.; Perinot, A.; Chen, Z.; Facchetti, A.; Caironi, M. Macroscopic and High-Throughput Printing of Aligned Nanostructured Polymer Semiconductors for MHz Large-Area Electronics. *Nat. Commun.* **2015**, *6*, 8394.

(14) Schott, S.; Gann, E.; Thomsen, L.; Jung, S.-H.; Lee, J.-K.; McNeill, C. R.; Sirringhaus, H. Charge-Transport Anisotropy in a Uniaxially Aligned Diketopyrrolopyrrole-Based Copolymer. *Adv. Mater.* **2015**, *27*, 7356.

(15) Wang, G.; Huang, W.; Eastham, N. D.; Fabiano, S.; Manley, E. F.; Zeng, L.; Wang, B.; Zhang, X.; Chen, Z.; Li, R.; Chang, R. P. H.;

DOI: 10.1021/acsami.9b20991
ACS Appl. Mater. Interfaces 2020, 12, 2753–2762

Chen, L. X.; Bedzyk, M. J.; Melkonyan, F. S.; Facchetti, A.; Marks, T. J. Aggregation control in natural brush-printed conjugated polymer films and implications for enhancing charge transport. *Proc. Natl. Acad. Sci. U.S.A.* **2017**, *114*, E10066−E10073.
(16) Khim, D.; Luzio, A.; Bonacchini, G. E.; Pace, G.; Lee, M.-J.; Noh, Y.-Y.; Caironi, M. Uniaxial Alignment of Conjugated Polymer Films for High-Performance Organic Field-Effect Transistors. *Adv. Mater.* **2018**, *30*, 1705463.
(17) Zhang, F.; Mohammadi, E.; Luo, X.; Strzalka, J.; Mei, J.; Diao, Y. Critical Role of Surface Energy in Guiding Crystallization of Solution-Coated Conjugated Polymer Thin Films. *Langmuir* **2018**, *34*, 1109−1122.
(18) Guo, D.-Y.; Tsai, Y.-b.; Yu, T.-F.; Lee, W.-Y. Interfacial effects on solution-sheared thin-film transistors. *J. Mater. Chem. C* **2018**, *6*, 12006−12015.
(19) Li, M.; An, C.; Marszalek, T.; Baumgarten, M.; Müllen, K.; Pisula, W. Impact of Interfacial Microstructure on Charge Carrier Transport in Solution-Processed Conjugated Polymer Field-Effect Transistors. *Adv. Mater.* **2016**, *28*, 2245−2252.
(20) Li, J.; Tang, W.; Wang, Q.; Sun, W.; Zhang, Q.; Guo, X.; Wang, X.; Yan, F. Solution-processable organic and hybrid gate dielectrics for printed electronics. *Mater. Sci. Eng., R* **2018**, *127*, 1−36.
(21) Wu, D.; Kaplan, M.; Ro, H. W.; Engmann, S.; Fischer, D. A.; DeLongchamp, D. M.; Richter, L. J.; Gann, E.; Thomsen, L.; McNeill, C. R.; Zhang, X. Blade Coating Aligned, High-Performance, Semiconducting-Polymer Transistors. *Chem. Mater.* **2018**, *30*, 1924−1936.
(22) Na, J. Y.; Kang, B.; Lee, S. G.; Cho, K.; Park, Y. D. Surface-Mediated Solidification of a Semiconducting Polymer during Time-Controlled Spin-Coating. *ACS Appl. Mater. Interfaces* **2017**, *9*, 9871−9879.
(23) Mohammadi, E.; Zhao, C.; Meng, Y.; Qu, G.; Zhang, F.; Zhao, X.; Mei, J.; Zuo, J.-M.; Shukla, D.; Diao, Y. Dynamic-template-directed multiscale assembly for large-area coating of highly-aligned conjugated polymer thin films. *Nat. Commun.* **2017**, *8*, 16070.
(24) Tseng, H.-R.; Ying, L.; Hsu, B. B. Y.; Perez, L. A.; Takacs, C. J.; Bazan, G. C.; Heeger, A. J. High Mobility Field Effect Transistors Based on Macroscopically Oriented Regioregular Copolymers. *Nano Lett.* **2012**, *12*, 6353−6357.
(25) Li, M.; Hinkel, F.; Müllen, K.; Pisula, W. Self-assembly and charge carrier transport of solution-processed conjugated polymer monolayers on dielectric surfaces with controlled sub-nanometer roughness. *Nanoscale* **2016**, *8*, 9211−9216.
(26) Mohammadi, E.; Qu, G.; Kafle, P.; Jung, S.-H.; Lee, J.-K.; Diao, Y. Design Rules for Dynamic-Template-Directed Crystallization of Conjugated Polymers. *Mol. Syst. Des. Eng.* **2020**, DOI: 10.1039/C9ME00042A.
(27) Mohammadi, E.; Zhao, C.; Zhang, F.; Qu, G.; Jung, S.-H.; Zhao, Q.; Evans, C. M.; Lee, J.-K.; Shukla, D.; Diao, Y. Ion Gel Dynamic Templates for Large Modulation of Morphology and Charge Transport Properties of Solution-Coated Conjugated Polymer Thin Films. *ACS Appl. Mater. Interfaces* **2019**, *11*, 22561−22574.
(28) Mammen, M.; Choi, S.-K.; Whitesides, G. M. Polyvalent Interactions in Biological Systems: Implications for Design and Use of Multivalent Ligands and Inhibitors. *Angew. Chem., Int. Ed.* **1998**, *37*, 2754−2794.
(29) Badjić, J. D.; Nelson, A.; Cantrill, S. J.; Turnbull, W. B.; Stoddart, J. F. Multivalency and Cooperativity in Supramolecular Chemistry. *Acc. Chem. Res.* **2005**, *38*, 723−732.
(30) Mulder, A.; Huskens, J.; Reinhoudt, D. N. Multivalency in supramolecular chemistry and nanofabrication. *Org. Biomol. Chem.* **2004**, *2*, 3409−3424.
(31) Hunter, C. A.; Anderson, H. L. What is Cooperativity? *Angew. Chem., Int. Ed.* **2009**, *48*, 7488−7499.
(32) Zhang, Y.; Yu, Y.; Jiang, Z.; Xu, H.; Wang, Z.; Zhang, X.; Oda, M.; Ishizuka, T.; Jiang, D.; Chi, L.; Fuchs, H. Single-Molecule Study on Intermolecular Interaction between C60 and Porphyrin Derivatives: Toward Understanding the Strength of the Multivalency. *Langmuir* **2009**, *25*, 6627−6632.
(33) Mahalingam, V.; Onclin, S.; Péter, M.; Ravoo, B. J.; Huskens, J.; Reinhoudt, D. N. Directed Self-Assembly of Functionalized Silica Nanoparticles on Molecular Printboards through Multivalent Supramolecular Interactions. *Langmuir* **2004**, *20*, 11756−11762.
(34) Di Palma, G.; Kotowska, A. M.; Hart, L. R.; Scurr, D. J.; Rawson, F. J.; Tommasone, S.; Mendes, P. M. Reversible, High-Affinity Surface Capturing of Proteins Directed by Supramolecular Assembly. *ACS Appl. Mater. Interfaces* **2019**, *11*, 8937−8944.
(35) Qu, G.; Zhao, X.; Newbloom, G. M.; Zhang, F.; Mohammadi, E.; Strzalka, J. W.; Pozzo, L. D.; Mei, J.; Diao, Y. Understanding Interfacial Alignment in Solution Coated Conjugated Polymer Thin Films. *ACS Appl. Mater. Interfaces* **2017**, *9*, 27863−27874.
(36) Köhler, A.; dos Santos, D. A.; Beljonne, D.; Shuai, Z.; Brédas, J.-L.; Holmes, A. B.; Kraus, A.; Müllen, K.; Friend, R. H. Charge Separation in Localized and Delocalized Electronic States in Polymeric Semiconductors. *Nature* **1998**, *392*, 903.
(37) Vezie, M. S.; Few, S.; Meager, I.; Pieridou, G.; Dörling, B.; Ashraf, R. S.; Goñi, A. R.; Bronstein, H.; McCulloch, I.; Hayes, S. C.; Campoy-Quiles, M.; Nelson, J. Exploring the Origin of High Optical Absorption in Conjugated Polymers. *Nat. Mater.* **2016**, *15*, 746.
(38) Spano, F. C.; Silva, C. H- and J-Aggregate Behavior in Polymeric Semiconductors. *Annu. Rev. Phys. Chem.* **2014**, *65*, 477−500.
(39) Park, K. S.; Kwok, J. J.; Dilmurat, R.; Qu, G.; Kafle, P.; Luo, X.; Jung, S.-H.; Olivier, Y.; Lee, J.-K.; Mei, J.; Beljonne, D.; Diao, Y. Tuning conformation, assembly, and charge transport properties of conjugated polymers by printing flow. *Sci. Adv.* **2019**, *5*, No. eaaw7757.
(40) Evans, C. M.; Bridges, C. R.; Sanoja, G. E.; Bartels, J.; Segalman, R. A. Role of Tethered Ion Placement on Polymerized Ionic Liquid Structure and Conductivity: Pendant versus Backbone Charge Placement. *ACS Macro Lett.* **2016**, *5*, 925−930.
(41) Ito, Y.; Virkar, A. A.; Mannsfeld, S.; Oh, J. H.; Toney, M.; Locklin, J.; Bao, Z. Crystalline Ultrasmooth Self-Assembled Monolayers of Alkylsilanes for Organic Field-Effect Transistors. *J. Am. Chem. Soc.* **2009**, *131*, 9396−9404.
(42) McCulloch, I.; Salleo, A.; Chabinyc, M. Avoid the kinks when measuring mobility. *Science* **2016**, *352*, 1521−1522.
(43) Choi, H. H.; Cho, K.; Frisbie, C. D.; Sirringhaus, H.; Podzorov, V. Critical assessment of charge mobility extraction in FETs. *Nat. Mater.* **2017**, *17*, 2.
(44) Zhang, X.; Richter, L. J.; DeLongchamp, D. M.; Kline, R. J.; Hammond, M. R.; McCulloch, I.; Heeney, M.; Ashraf, R. S.; Smith, J. N.; Anthopoulos, T. D.; Schroeder, B.; Geerts, Y. H.; Fischer, D. A.; Toney, M. F. Molecular Packing of High-Mobility Diketo Pyrrolo-Pyrrole Polymer Semiconductors with Branched Alkyl Side Chains. *J. Am. Chem. Soc.* **2011**, *133*, 15073−15084.
(45) Silverstein, R. M.; Bassler, G. C. Spectrometric identification of organic compounds. *J. Chem. Educ.* **1962**, *39*, 546.
(46) Höfft, O.; Bahr, S.; Kempter, V. Investigations with Infrared Spectroscopy on Films of the Ionic Liquid [EMIM]Tf2N. *Langmuir* **2008**, *24*, 11562−11566.
(47) Zhang, F.; Di, C.-a.; Berdunov, N.; Hu, Y.; Hu, Y.; Gao, X.; Meng, Q.; Sirringhaus, H.; Zhu, D. Ultrathin Film Organic Transistors: Precise Control of Semiconductor Thickness via Spin-Coating. *Adv. Mater.* **2013**, *25*, 1401−1407.
(48) Schneider, C. A.; Rasband, W. S.; Eliceiri, K. W. NIH Image to ImageJ: 25 years of image analysis. *Nat. Methods* **2012**, *9*, 671.
(49) Jiang, Z.; Li, X.; Strzalka, J.; Sprung, M.; Sun, T.; Sandy, A. R.; Narayanan, S.; Lee, D. R.; Wang, J. The dedicated high-resolution grazing-incidence X-ray scattering beamline 8-ID-E at the Advanced Photon Source. *J. Synchrotron Radiat.* **2012**, *19*, 627−636.

DOI: 10.1021/acsami.9b20991
ACS Appl. Mater. Interfaces 2020, 12, 2753−2762